

PRESSURE-ROBUSTNESS FOR THE AXISYMMETRIC STOKES PROBLEM BY VELOCITY RECONSTRUCTION

P.L. LEDERER^{*}, C. LEHRENFELD[†], C. MERDON[‡], AND T. VAN BEECK[†]

Abstract. This paper studies pressure-robustness for the axisymmetric Stokes problem. The transformation to cylindrical coordinates requires that the radially weighted velocity is divergence-free in the classical sense. Consequently, traditional divergence-free finite element methods from the Cartesian setting – even if inf-sup stable – are in general not divergence-free in the axisymmetric formulation.

We therefore explore the approach that restores pressure-robustness via reconstruction operators for a low-order Bernardi–Raugel discretization. We show that an application of standard interpolation operators from the Cartesian setting to radially weighted test functions works in principle, but it lacks properties needed to derive optimal consistency error estimates.

To address this, we introduce a reconstruction operator into a finite element space spanned by Raviart–Thomas functions that are modified such that they vanish on the rotation axis. This vanishing-on-axis property is the key to obtain optimal consistency error estimates. Numerical examples demonstrate the overall feasibility of the approach and include cases where the vanishing-on-axis property yields significantly better results.

Key words. Axisymmetric Stokes problem, Pressure-robustness, Bernardi–Raugel finite element method, Mass conservation

MSC codes. 65N30, 76M10, 65N12, 76D07

1. Introduction. In recent years, pressure-robustness has become a major point of focus in the numerical analysis of the incompressible (Navier–) Stokes equations [9]. Examples of pressure-robust discretizations are based on finite elements providing exactly divergence-free velocities, such as the Scott–Vogelius element [23, 24] or $H(\text{div})$ -conforming (hybrid) discontinuous Galerkin methods [4, 14, 8, 21]. Another approach is the use of a velocity reconstruction operator [15, 17, 11, 9] applied to test functions. All of these schemes work in the two- and three-dimensional setting.

When the domain, data, and solution are rotationally invariant, the original three-dimensional problem can be reduced to a two-dimensional axisymmetric formulation, which can be solved at a significantly lower computational cost. Unfortunately, without further modifications, classical pressure-robust schemes lose their pressure-robustness under the associated change of variables. To be precise, let Ω denote the two-dimensional meridional (r, z) -domain and let $\hat{\Omega}$ be the three-dimensional domain obtained by revolving Ω about the rotation axis. We consider the three-dimensional Stokes problem: find $\mathbf{u} : \hat{\Omega} \subset \mathbb{R}^3 \rightarrow \mathbb{R}^3$ such that

$$(1.1) \quad -\nu \Delta \mathbf{u} + \nabla p = f \quad \text{in } \hat{\Omega},$$

$$(1.2) \quad \text{div } \mathbf{u} = 0 \quad \text{in } \hat{\Omega},$$

$$(1.3) \quad \mathbf{u} = 0 \quad \text{on } \partial \hat{\Omega}.$$

Transforming to cylindrical coordinates (r, θ, z) and assuming that the problem is axisymmetric, i.e. independent of θ , we obtain a mixed problem of the form: find

^{*}Department of Mathematics, University of Hamburg, Bundesstraße 55, D-20146 Hamburg, Germany (philip.leder@uni-hamburg.de).

[†]Institute for Numerical and Applied Mathematics, University of Göttingen, Lotzestraße 16-18, D-37083 Göttingen, Germany (lehrenfeld@math.uni-goettingen.de, t.beeck@math.uni-goettingen.de).

[‡]Weierstrass Institute for Applied Analysis and Stochastics (WIAS), Anton-Wilhelm-Amo-Straße 39, D-10117 Berlin, Germany (christian.merdon@wias-berlin.de).

$\mathbf{u} \in \mathbf{V}$ and $p \in Q$ – with \mathbf{V} and Q being appropriate function spaces for velocity and pressure on Ω , respectively – such that

$$\begin{aligned} \nu a(\mathbf{u}, \mathbf{v}) + b(p, \mathbf{v}) &= (\mathbf{f}, r\mathbf{v})_{L^2} & \text{for all } \mathbf{v} \in \mathbf{V}, \\ b(q, \mathbf{u}) &= 0 & \text{for all } q \in Q, \end{aligned}$$

with the standard L^2 -inner product $(\cdot, \cdot)_{L^2}$ (i.e. without a weighting factor) over Ω and the bilinear forms

$$a(\mathbf{u}, \mathbf{v}) := (r\nabla_{(r,z)}\mathbf{u}, \nabla_{(r,z)}\mathbf{v})_{L^2} + (r^{-2}u_r, v_r)_{L^2}, \quad b(q, \mathbf{v}) := (\operatorname{div}_{(r,z)}(r\mathbf{v}), q)_{L^2}.$$

Here, the operators $\nabla_{(r,z)}$ and $\operatorname{div}_{(r,z)}$ denote the standard gradient and divergence with respect to the (r, z) coordinates and \cdot_r refers to the radial component, see e.g. [1] for a proper derivation of the above formulation. The forms $a(\cdot, \cdot)$ and $b(\cdot, \cdot)$ differ from the usual Stokes forms in Cartesian coordinates. At first glance, the change looks minor, but the divergence operator’s structure changes significantly under the cylindrical-coordinate transform. For instance, because of the additional radial factor r one would now require $\operatorname{div}_{(r,z)}(r\mathbf{V}_h) \subseteq Q_h$ to obtain an *exactly* divergence-free discretization. Consequently, well-known exactly divergence-free velocity ansatz spaces, e.g. those provided by the Scott–Vogelius finite element, do not satisfy this property and therefore do not yield a pressure-robust method; we illustrate this in Figure 1. A related phenomenon was observed in [20] for an acoustic eigenvalue problem, where the axisymmetric transform produces spurious eigenmodes.

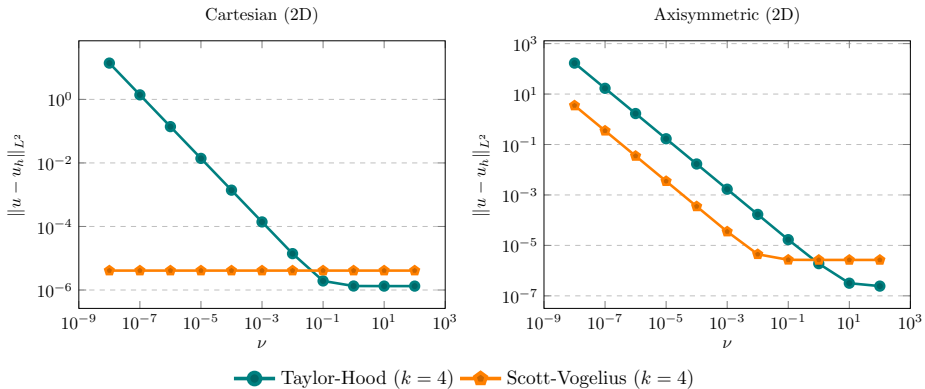


Figure 1: Illustrating pressure-robustness for the Taylor–Hood and Scott–Vogelius pairs in Cartesian (left) and axisymmetric (right) settings for right-hand sides $\mathbf{f} = -\nu\Delta\mathbf{u} + \nabla p$. A pressure-robust method yields ν -independent velocity errors, whereas non-robust methods show locking w.r.t. ν . Taylor–Hood is not pressure-robust and Scott–Vogelius is only pressure-robust in the Cartesian setting. In this example, \mathbf{f} is computed from $\mathbf{u} = \operatorname{curl}(x^2(x-1)^2y^2(y-1)^2)$ and $p = x^5 + y^5 - \frac{1}{3}$ in the Cartesian case, and as in Section 6.2 in the axisymmetric case.

Another difficulty stems from the r^{-1} weights in the bilinear form $a(\cdot, \cdot)$: they require that the radial component u_r vanish at the rotation axis, which is natural for radially symmetric flows but complicates discretizations with $H(\operatorname{div})$ -conforming ansatz spaces. To the best of the authors’ knowledge, only a few exactly divergence-free discretizations on structured meshes are available [3, 19].

Furthermore, deriving inf-sup stability of a finite element pair from the three-dimensional setting is not straightforward; see [12, 13] for the Taylor–Hood and [22] for the P2-bubble finite element method.

This paper employs a classical low-order Bernardi–Raugel finite element discretization [2] and modifies it with the help of a reconstruction operator in the spirit of [15, 17, 11, 9] to achieve pressure-robustness. We present the Bernardi–Raugel pair here as the first axisymmetric pressure-robust scheme on unstructured grids and as a prototype that paves the way for a broader class of pressure-robust axisymmetric discretizations.

All considered reconstruction operators Π map discretely divergence-free test functions to exactly divergence-free $H(\text{div})$ -conforming ones by utilizing the commutative property $\text{div}_{(r,z)}\Pi(r\mathbf{v}_h) = \pi_0\text{div}_{(r,z)}(r\mathbf{v}_h)$. Two approaches are discussed. The first one employs classical $H(\text{div})$ -conforming standard interpolations, that are only guaranteed to work under higher regularity assumptions on the problem data. To fix this flaw, a second approach employs a modified $H(\text{div})$ -conforming finite element space that guarantees that also the tangential component of the reconstructed functions $r\mathbf{v}_h$ vanish at the rotation axis. This property allows L^2_{-1} estimates of the reconstructions and is the key for an improved and optimal consistency error estimate. The theoretical results and the properties of the modified reconstruction operators are confirmed in several numerical experiments. Moreover, the reconstruction operator applied to the discrete velocity solution is divergence-free (in the sense above) and can be used in coupled axisymmetric transport simulations to guarantee maximum principles and mass conservation [7].

Furthermore, the reconstruction space motivates $H(\text{div})$ -conforming (H)-DG in the spirit of [4, 14, 8, 21]. A thorough investigation of this possibility is the topic of a forthcoming paper.

The remaining parts of this paper are structured as follows. Section 2 studies the well-posedness of the axisymmetric Stokes model problem and introduces the necessary notation. Section 3 introduces the concept of pressure-robustness, derives a general a priori error estimate and investigates the employment of traditional $H(\text{div})$ -conforming standard interpolations. Section 5 suggests a modification of the reconstruction operator that allows for an improved consistency error estimate and optimal a priori velocity error estimates without additional regularity assumptions. Section 6 presents several numerical examples to confirm the results.

2. Model problem and preliminaries. This section fixes the notation for the axisymmetric setting and recalls the strong and weak formulation, as well as the Helmholtz decomposition.

2.1. Axisymmetric geometry. Let $\Omega \subset \mathbb{R}_+ \times \mathbb{R}$, where \mathbb{R}_+ are the non-negative real numbers, be a Lipschitz domain that generates a domain $\hat{\Omega} \subset \mathbb{R}^3$ through rotation around a rotation axis $\Gamma_{\text{rot}} \subset \partial\Omega$. We denote by (x, y, z) a set of Cartesian coordinates in \mathbb{R}^3 and by (r, θ, z) , $r \geq 0$, $\theta \in [0, 2\pi]$, the associated cylindrical coordinates such that $x = r \cos \theta$ and $y = r \sin \theta$. We assume that

$$\Gamma_{\text{rot}} = \{(r, z) \in \Omega : r = 0\}, \quad \text{and} \quad \hat{\Omega} = \{(r \cos \theta, r \sin \theta, z) : (r, z) \in \Omega, \theta \in [0, 2\pi]\}.$$

In the following, we set $\Gamma := \partial\Omega \setminus \Gamma_{\text{rot}}$. The geometric setup is visualized in Figure 2. For any vector, or vector-valued function \mathbf{v} , we denote by (v_x, v_y, v_z) and (v_r, v_θ, v_z) its components in the Cartesian and cylindrical coordinate system, respectively. In this work we only consider the axisymmetric case, i.e. $v_\theta = 0$ and all functions are

independent of the angular coordinate θ . For simplicity we then only consider the two-dimensional vector $\mathbf{v} = (v_r, v_z)$ in the (r, z) -plane.

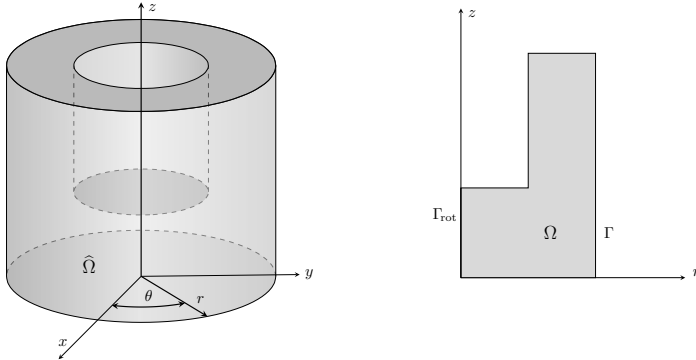


Figure 2: Geometric setup: the two-dimensional meridional domain Ω (right) and its revolution about the rotation axis Γ_{rot} generate the three-dimensional domain $\widehat{\Omega}$ (left). The boundary Γ denotes the non-axis portion of $\partial\Omega$.

2.2. Strong formulation and differential operators. Considering homogeneous Dirichlet boundary conditions, the strong form of the axisymmetric Stokes problem seeks $\mathbf{u} = (u_r, u_z)$ and p such that

$$\begin{aligned} \nu \Delta_{\text{axi}} \mathbf{u} + \nabla p &= \mathbf{f} & \text{in } \Omega, \\ \text{div}_{\text{axi}} \mathbf{u} &= 0 & \text{in } \Omega, \\ \mathbf{u} &= \mathbf{0} & \text{on } \Gamma, \end{aligned}$$

and involves the axisymmetric vector Laplacian and divergence operator

$$\Delta_{\text{axi}} \mathbf{u} := \begin{pmatrix} \Delta_{(r,z)} u_r + \frac{1}{r} \partial_r u_r - r^{-2} u_r \\ \Delta_{(r,z)} u_z + \frac{1}{r} \partial_r u_z \end{pmatrix} \quad \text{and} \quad \text{div}_{\text{axi}} := \text{div}_{(r,z)}(\mathbf{v}) + r^{-1} v_r.$$

Here and throughout

$$\Delta_{(r,z)} v := \partial_r^2 v + \partial_z^2 v, \quad \nabla_{(r,z)} \mathbf{v} := (\partial_r v_r, \partial_z v_z), \quad \text{and} \quad \text{div}_{(r,z)} \mathbf{v} := \partial_r v_r + \partial_z v_z,$$

denote the classical differential operators known from the Cartesian setting but with respect to the cylindrical coordinates (r, z) . Note that non-homogeneous Dirichlet boundary conditions can be treated in a standard way via homogenization.

2.3. Weak formulation and weighted Sobolev spaces. The weak formulation employs weighted Sobolev spaces $L_s^2(\Omega)$ and $H_s^1(\Omega)$, see [10, 1, 6], that are Hilbert spaces with the inner products

$$(p, q)_{L_s^2} := \int_{\Omega} r^s p q \, dr dz, \quad \text{and} \quad (p, q)_{H_s^1} := \int_{\Omega} r^s (p q + \nabla p \cdot \nabla q) \, dr dz,$$

and the corresponding weighted norms $\|q\|_{L_s^2}^2 := (q, q)_{L_s^2}$ and $\|q\|_{H_s^1}^2 := (q, q)_{H_s^1}$, respectively. We omit the index s in the notation if $s = 0$.

The weak solution $(\mathbf{u}, p) \in \mathbf{V} \times Q$ of the axisymmetric Stokes solves the mixed problem

$$(2.1a) \quad \nu a(\mathbf{u}, \mathbf{v}) + b(p, \mathbf{v}) = (\mathbf{f}, r\mathbf{v})_{L^2} \quad \text{for all } \mathbf{v} \in \mathbf{V},$$

$$(2.1b) \quad b(q, \mathbf{u}) = 0 \quad \text{for all } q \in Q,$$

where the bilinear forms read

$$a(\mathbf{u}, \mathbf{v}) := (\nabla_{(r,z)} \mathbf{u}, \nabla_{(r,z)} \mathbf{v})_{L^2_1} + (u_r, v_r)_{L^2_{-1}} \quad \text{and} \quad b(q, \mathbf{v}) := (\operatorname{div}_{(r,z)}(r\mathbf{v}), q)_{L^2}.$$

The space $\mathbf{V} := \{v \in \mathbf{H}^1_1(\Omega) : v_r \in L^2_{-1}(\Omega)\}$ is equipped with the inner product $a(\cdot, \cdot)$ and corresponding energy norm

$$\|\mathbf{v}\|_{\mathbf{V}}^2 := a(\mathbf{v}, \mathbf{v}) = \|\nabla \mathbf{v}\|_{L^2_1}^2 + \|v_r\|_{L^2_{-1}}^2.$$

Observe, that boundedness in the energy norm requires $v_r = 0$ along the rotation axis Γ_{rot} (if it is part of the domain boundary). On the remaining boundary $\Gamma := \partial\Omega \setminus \Gamma_{\text{rot}}$, homogeneous Dirichlet boundary conditions are assumed for simplicity. The pressure space $Q := \{q \in L^2_1(\Omega) : \int_{\Omega} r q dx = 0\}$ fixes the integral mean to ensure uniqueness. Well-posedness is inherited from the three-dimensional setting via the transformations in Remark 2.1 below. More details on the functional analysis and well-posedness for axisymmetric problems can be found in [1].

In the axisymmetric setting, it is the flux quantity $r\mathbf{u}$ that is conserved and hence divergence-free. With abuse of notation we denote the corresponding velocity \mathbf{u} as divergence-free in the sense that

$$\mathbf{u} \in \mathbf{V}_0 := \{\mathbf{v} \in \mathbf{V} : b(\mathbf{v}, q) = 0 \text{ for all } q \in Q\}.$$

We denote the $a(\cdot, \cdot)$ -orthogonal complement to \mathbf{V}_0 in \mathbf{V} by \mathbf{V}_{\perp} , i.e. $\mathbf{V} = \mathbf{V}_0 \oplus_a \mathbf{V}_{\perp}$. Motivated by the continuity estimate

$$b(q, \mathbf{v}) = (\operatorname{div}_{(r,z)}(r\mathbf{v}), q)_{L^2} \leq \|\operatorname{div}_{(r,z)}(r\mathbf{v})\|_{L^2_{-1}} \|q\|_{L^2_1} \quad \text{for all } \mathbf{v} \in \mathbf{V}, q \in Q,$$

and

$$(2.2) \quad \begin{aligned} \|\operatorname{div}_{(r,z)}(r\mathbf{v})\|_{L^2_{-1}}^2 &= \int_{\Omega} r^{-1} (\operatorname{div}_{(r,z)}(r\mathbf{v}))^2 \operatorname{drdz} = \int_{\Omega} r^{-1} (r \operatorname{div}_{(r,z)}(\mathbf{v}) + v_r)^2 \operatorname{drdz}, \\ &\leq 2 \int_{\Omega} r (\operatorname{div}_{(r,z)}(\mathbf{v}))^2 \operatorname{drdz} + 2 \int_{\Omega} r^{-1} v_r^2 \operatorname{drdz} \lesssim \|\mathbf{v}\|_{\mathbf{V}}^2, \end{aligned}$$

we further see that

$$(2.3) \quad r\mathbf{u} \in H_{-1}(\operatorname{div}, \Omega) := \left\{ \mathbf{v} \in L^2_{-1}(\Omega) : \operatorname{div}_{(r,z)}(\mathbf{v}) \in L^2_{-1}(\Omega) \right\}.$$

Here and in the following we omit the subscript (r, z) of the divergence in the notation of the $H_{-1}(\operatorname{div}, \Omega)$ -space (and similar ones) for brevity.

Sections 4 and 5 discuss pressure-robust finite element discretizations that are based on reconstructions of the weighted (discrete) test functions $r\mathbf{v}_h$. The most sophisticated approach, as it allows for an error analysis with improved consistency error, is motivated by (2.3) but is weakened in the sense that it only maps into

$$(2.4) \quad L^2_{-1}(\Omega) \cap H(\operatorname{div}, \Omega) = \left\{ \mathbf{v} \in L^2_{-1}(\Omega) : \operatorname{div}_{(r,z)}(\mathbf{v}) \in L^2(\Omega) \right\}.$$

Thus, we only consider standard $H(\operatorname{div})$ -conformity without the weighting factor r in the norm-bound of the divergence.

Remark 2.1 (Transformation to the three-dimensional setting). Note that the bilinear forms are equivalent to the bilinear forms of the three-dimensional Stokes problem in Cartesian coordinates on the body of revolution $\widehat{\Omega}$ (up to a factor 2π) by the transformation rules

$$a(\mathbf{u}, \mathbf{v}) = \int_{\Omega} \left(\nabla \mathbf{u} : \nabla \mathbf{v} + r^{-2} u_r v_r \right) r \, dr dz = \frac{1}{2\pi} \int_{\widehat{\Omega}} \nabla_{\widehat{\mathbf{x}}} \widehat{\mathbf{u}} : \nabla_{\widehat{\mathbf{x}}} \widehat{\mathbf{v}} \, d\widehat{\mathbf{x}},$$

and

$$b(q, \mathbf{v}) = (\operatorname{div}_{(r,z)}(r\mathbf{v}), q)_{L^2} = \int_{\Omega} q \left(\operatorname{div}_{(r,z)}(\mathbf{v}) + r^{-1} v_r \right) r \, dr dz = \frac{1}{2\pi} \int_{\widehat{\Omega}} \widehat{q} \operatorname{div}_{\widehat{\mathbf{x}}}(\widehat{\mathbf{v}}) \, d\widehat{\mathbf{x}}.$$

2.4. Helmholtz projection. The Helmholtz decomposition splits any axisymmetric forcing into a gradient (pressure) part and a divergence-free remainder. Concretely, for any $\mathbf{f} \in L_1^2(\Omega)$ there exist

$$(2.5) \quad \mathbf{f} = \nabla \alpha_{\mathbf{f}} + \mathbb{P}\mathbf{f},$$

with $\alpha_{\mathbf{f}} \in H_1^1(\Omega)/\mathbb{R}$ determined by

$$(\nabla \alpha_{\mathbf{f}}, \nabla \beta)_{L_1^2} = (\mathbf{f}, \nabla \beta)_{L_1^2} \quad \text{for all } \beta \in H_1^1(\Omega)/\mathbb{R}.$$

The remainder $\mathbb{P}\mathbf{f}$ is L_1^2 -orthogonal to all gradients, i.e. $(\mathbb{P}\mathbf{f}, \nabla q)_{L_1^2} = 0$ for all $q \in H_1^1(\Omega)$. Furthermore, $\nabla \alpha_{\mathbf{f}}$ is L_1^2 -orthogonal to all divergence-free functions $\mathbf{v}_0 \in \mathbf{V}_0$, since

$$(\nabla \alpha_{\mathbf{f}}, \mathbf{v}_0)_{L_1^2} = (\nabla \alpha_{\mathbf{f}}, r\mathbf{v}_0)_{L^2} = (\alpha_{\mathbf{f}}, \operatorname{div}_{(r,z)}(r\mathbf{v}_0))_{L^2} = 0.$$

We extend the Helmholtz projector to duals $\mathbf{g} \in \mathbf{V}^*$ by restriction to the divergence-free subspace \mathbf{V}_0 : for $\mathbf{v} \in \mathbf{V}$ with $\mathbf{v} = \mathbf{v}_0 + \mathbf{v}_{\perp}$, $\mathbf{v}_0 \in \mathbf{V}_0$, $\mathbf{v}_{\perp} \in \mathbf{V}_{\perp}$, set

$$\langle \mathbb{P}\mathbf{g}, \mathbf{v} \rangle_{\mathbf{V}^* \times \mathbf{V}} := \langle \mathbf{g}, \mathbf{v}_0 \rangle_{\mathbf{V}^* \times \mathbf{V}}.$$

If the functional $\mathbf{g} \in \mathbf{V}^*$ is represented by a field $\mathbf{f} \in L_1^2(\Omega)$ then $\mathbb{P}\mathbf{g}$ coincides with $\mathbb{P}\mathbf{f} \in L_1^2(\Omega)$, since

$$\langle \mathbf{g}, \mathbf{v}_0 \rangle_{\mathbf{V}^* \times \mathbf{V}} = (\mathbf{f}, \mathbf{v}_0)_{L^2} = (\nabla \alpha_{\mathbf{f}}, \mathbf{v}_0)_{L_1^2} + (\mathbb{P}\mathbf{f}, \mathbf{v}_0)_{L_1^2} = (\mathbb{P}\mathbf{f}, \mathbf{v}_0)_{L_1^2} \quad \text{for all } \mathbf{v}_0 \in \mathbf{V}_0,$$

by orthogonality of $\nabla \alpha_{\mathbf{f}}$ to \mathbf{V}_0 . An important application is $\mathbf{g} = -\Delta_{\text{axi}} \mathbf{u} \in \mathbf{V}^*$, defined via

$$(2.6) \quad \langle -\Delta_{\text{axi}} \mathbf{u}, \mathbf{v} \rangle_{\mathbf{V}^* \times \mathbf{V}} := a(\mathbf{u}, \mathbf{v}) \quad \text{for all } \mathbf{v} \in \mathbf{V}.$$

Testing this identity with $\mathbf{v}_0 \in \mathbf{V}_0$ gives

$$\langle \mathbb{P}(-\Delta_{\text{axi}} \mathbf{u}), \mathbf{v}_0 \rangle = a(\mathbf{u}, \mathbf{v}_0) = \frac{1}{\nu} (\mathbf{f}, \mathbf{v}_0)_{L_1^2} = \frac{1}{\nu} (\mathbb{P}\mathbf{f}, \mathbf{v}_0)_{L_1^2}.$$

Hence, even if $-\Delta_{\text{axi}} \mathbf{u}$ need not lie in $L_1^2(\Omega)$, its Helmholtz projection has the L_1^2 -representation $\nu^{-1} \mathbb{P}\mathbf{f}$.

3. Pressure-robustness for the axisymmetric Stokes problem by reconstruction operators. In the Cartesian setting, pressure-robustness of a non-divergence-free method can be achieved by applying a reconstruction operator to the right-hand side, see [15, 16, 17, 11]. The main idea is to replace the discretely divergence-free test functions with exactly divergence-free ones that are conforming at least in an $H(\operatorname{div})$ sense. In this section, we study the application of a generic reconstruction operator to radially-weighted test functions in the axisymmetric setting.

3.1. A modified finite element method. Consider a regular triangulation \mathcal{T} of Ω into triangles with vertices \mathcal{N} and edges \mathcal{E} , and let $P_k(\mathcal{T})$ be the space of piecewise polynomials of order k . We assume at least the regularity $\mathbf{f} \in L_1^2(\Omega)$, corresponding to $\hat{\mathbf{f}} \in L^2(\hat{\Omega})$ in the three-dimensional transformed problem. The modified axisymmetric Stokes problem seeks $(\mathbf{u}_h, p_h) \in \mathbf{V}_h \times Q_h$, such that

$$(3.1a) \quad \nu a(\mathbf{u}_h, \mathbf{v}_h) + b(p_h, \mathbf{v}_h) = (\mathbf{f}, \Pi(r\mathbf{v}_h))_{L^2} \quad \text{for all } \mathbf{v}_h \in \mathbf{V}_h,$$

$$(3.1b) \quad b(q_h, \mathbf{u}_h) = 0 \quad \text{for all } q_h \in Q_h,$$

where Π is a suitable reconstruction operator. Note that with the choice $\Pi = \mathbb{I}$ (identity operator), we recover the classical finite element method without modifications.

The well-posedness of the problem hinges on the inf-sup stability of the pair $\mathbf{V}_h \times Q_h$ and the continuity of the modified right-hand side. For the latter, it suffices that the reconstruction operator provides the continuity estimate

$$(3.2) \quad \|\Pi(r\mathbf{v}_h)\|_{L_{-1}^2} \lesssim \|\mathbf{v}_h\|_{\mathbf{V}} \quad \text{for all } \mathbf{v}_h \in \mathbf{V}_h,$$

which then gives for $\mathbf{f} \in L_1^2(\Omega)$

$$(3.3) \quad (\mathbf{f}, \Pi(r\mathbf{v}_h))_{L^2} \leq \|\mathbf{f}\|_{L_1^2} \|\Pi(r\mathbf{v}_h)\|_{L_{-1}^2} \leq \|\mathbf{f}\|_{L_1^2} \|\mathbf{v}_h\|_{\mathbf{V}}.$$

Here, we consider the lowest-order Bernardi–Raugel finite element method with the velocity and pressure ansatz spaces

$$\mathbf{V}_h := \mathbf{P}_1(\mathcal{T}) \cup \{\lambda_i \lambda_j \mathbf{n}_E : E = \text{conv}\{P_i, P_j\} \in \mathcal{E}\}, \quad Q_h := P_0(\mathcal{T}) \cap L_{1,0}^2(\Omega).$$

Here, λ_j is the barycentric coordinate for the vertex P_j and \mathbf{n}_E is a fixed unit normal vector of the edge $E \in \mathcal{E}$. The space of discretely divergence-free functions is then given by

$$\mathbf{V}_{h,0} := \{\mathbf{v}_h \in \mathbf{V}_h : b(q_h, \mathbf{v}_h) = 0 \text{ for all } q_h \in Q_h\}.$$

The inf-sup stability of this pair can be shown, similar to the proof in [12, Section 2.2.1] for the Taylor–Hood finite element method, by using Scott–Zhang type quasi-interpolators to design a Fortin interpolator. Details can be found in [7].

Motivated by [17], a straightforward choice is the standard interpolation into the $\text{RT}_0(\mathcal{T})$ and $\text{BDM}_1(\mathcal{T})$ finite element spaces defined in Section 4. As these choices have some drawbacks, some enhancement is discussed in Section 5. Before that, this section concludes with some abstract a priori error estimates.

3.2. A priori error estimates. The following abstract a priori error estimate includes consistency errors caused by the application or non-application of a reconstruction operator Π in (3.1), which we estimate further in the following sections.

Apart from the Helmholtz decomposition of the right-hand side \mathbf{f} from (2.5), the analysis utilizes the discrete Stokes projector Π_S and the continuous Stokes lifting \mathcal{L}_S defined via

$$\begin{aligned} a(\Pi_S \mathbf{v}, \mathbf{v}_h) &= a(\mathbf{v}, \mathbf{v}_h) \quad \text{for all } \mathbf{v}_h \in \mathbf{V}_{h,0}, \mathbf{v} \in \mathbf{V}, \\ a(\mathcal{L}_S \mathbf{v}_h, \mathbf{v}) &= a(\mathbf{v}_h, \mathbf{v}) \quad \text{for all } \mathbf{v} \in \mathbf{V}_0, \mathbf{v}_h \in \mathbf{V}_h. \end{aligned}$$

Observe that there holds

$$(3.4) \quad a(\Pi_S \mathbf{v}, \mathbf{w}_h) = a(\mathbf{v}, \mathbf{w}_h) = a(\mathbf{v}, \mathcal{L}_S \mathbf{w}_h) \quad \text{for all } \mathbf{v} \in \mathbf{V}, \mathbf{w}_h \in \mathbf{V}_h.$$

Under some common regularity assumption, the lifting allows for the following error estimate.

LEMMA 3.1. *If the Stokes problem inherits $\mathbf{H}_1^{1+s}(\Omega) \times H_1^s(\Omega)$ elliptic regularity for some $s \in (0, 1]$ (from the equivalent three-dimensional problem) such that $\nu \|\mathbf{u}\|_{\mathbf{H}_1^{1+s}} + \|p\|_{H_1^s} \lesssim \|\mathbf{f}\|_{L_1^2}$, there holds*

$$\|\mathbf{w}_h - \mathcal{L}_S \mathbf{w}_h\|_{L_1^2} \lesssim h^s \|\operatorname{div}(r\mathbf{w}_h)\|_{L_{-1}^2} \lesssim h^s \|\mathbf{w}_h\|_{\mathbf{V}} \quad \text{for all } \mathbf{w}_h \in \mathbf{V}_h.$$

Proof. The proof follows the proof from [18, Lemma 5.2]. Let (ψ, λ) denote the solution of the axisymmetric Stokes problem

$$\begin{aligned} a(\psi, \mathbf{z}) + b(\lambda, \mathbf{z}) &= (\mathbf{w}_h - \mathcal{L}_S \mathbf{w}_h, \mathbf{z})_{L_1^2} \quad \text{for all } \mathbf{z} \in \mathbf{V}, \\ b(q, \psi) &= 0 \quad \text{for all } q \in Q. \end{aligned}$$

Testing with $\mathbf{z} = \mathbf{w}_h - \mathcal{L}_S \mathbf{w}_h$, using the definition of \mathcal{L}_S and inserting $\pi_{Q_h} \lambda$, i.e. the L_1^2 best approximation of λ in Q_h , yields

$$\begin{aligned} \|\mathbf{w}_h - \mathcal{L}_S \mathbf{w}_h\|_{L_1^2}^2 &= a(\psi, \mathbf{w}_h - \mathcal{L}_S \mathbf{w}_h) + b(\lambda, \mathbf{w}_h - \mathcal{L}_S \mathbf{w}_h) \\ &= b(\lambda, \Pi_S \mathbf{w}_h) \\ &= b(\lambda - \pi_{Q_h} \lambda, \Pi_S \mathbf{w}_h) \\ &\lesssim \|\lambda - \pi_{Q_h} \lambda\|_{L_1^2} \|\operatorname{div}(r\mathbf{w}_h)\|_{L_{-1}^2} \lesssim h^s \|\operatorname{div}(r\mathbf{w}_h)\|_{L_{-1}^2}. \end{aligned}$$

This and a similar estimate as in (2.2) concludes the proof. \square

We can show that the approximation error is bounded by the best-approximation error in $\mathbf{V}_{h,0}$, the L_1^2 -norm of the Helmholtz projector of $\Delta_{\text{axi}} \mathbf{u}$, and a *consistency error* defined as follows:

$$(3.5) \quad \mathcal{R}_\Pi := \|\mathbb{P}(\Delta_{\text{axi}} \mathbf{u}) \circ (\mathbb{I} - \Pi)\|_{\mathbf{V}_{h,0}^*} + \nu^{-1} \|\nabla \alpha_{\mathbf{f}} \circ \Pi\|_{\mathbf{V}_{h,0}^*}.$$

Here, the dual norms are defined as

$$(3.6) \quad \|\mathbb{P}(\Delta_{\text{axi}} \mathbf{u}) \circ (\mathbb{I} - \Pi)\|_{\mathbf{V}_{h,0}^*} := \sup_{\mathbf{w}_h \in \mathbf{V}_{h,0}} \frac{(\mathbb{P}(\Delta_{\text{axi}} \mathbf{u}), r\mathbf{w}_h - \Pi(r\mathbf{w}_h))_{L^2}}{\|\mathbf{w}_h\|_{\mathbf{V}}},$$

$$(3.7) \quad \|\nabla \alpha_{\mathbf{f}} \circ \Pi\|_{\mathbf{V}_{h,0}^*} := \sup_{\mathbf{w}_h \in \mathbf{V}_{h,0}} \frac{(\nabla \alpha_{\mathbf{f}}, \Pi(r\mathbf{w}_h))_{L^2}}{\|\mathbf{w}_h\|_{\mathbf{V}}},$$

where $\mathbb{P}(\Delta_{\text{axi}} \mathbf{u})$ is identified with its representation $-\nu^{-1} \mathbb{P} \mathbf{f} \in L_1^2(\Omega)$ as discussed at the end of Section 2.4, and $\nabla \alpha_{\mathbf{f}}$ is the remainder in the Helmholtz decomposition (2.5) of \mathbf{f} .

THEOREM 3.2 (A priori error estimate). *In addition to the assumptions of Lemma 3.1, we assume that $\mathbf{f} \in L_1^2(\Omega)$ and that Π allows for the continuity estimate (3.2). Then, the error between the exact velocity $\mathbf{u} \in \mathbf{V}$ solving (2.1) and the discrete velocity $\mathbf{u}_h \in \mathbf{V}_h$ solving (3.1) is bounded by*

$$\|\mathbf{u} - \mathbf{u}_h\|_{\mathbf{V}} \lesssim \inf_{\mathbf{v}_h \in \mathbf{V}_h^0} \|\mathbf{u} - \mathbf{v}_h\|_{\mathbf{V}} + h^s \|\mathbb{P}(\Delta_{\text{axi}} \mathbf{u})\|_{L_1^2} + \mathcal{R}_\Pi.$$

Proof. By definition of the discrete Stokes projector, the error can be split into a best-approximation error and a consistency error via the Pythagorean identity

$$\|\mathbf{u} - \mathbf{u}_h\|_{\mathbf{V}}^2 = \inf_{\mathbf{v}_h \in \mathbf{V}_h} \|\mathbf{u} - \mathbf{v}_h\|_{\mathbf{V}}^2 + \|\Pi_S \mathbf{u} - \mathbf{u}_h\|_{\mathbf{V}}^2.$$

Since $\mathbf{w}_h := \Pi_S \mathbf{u} - \mathbf{u}_h \in \mathbf{V}_{h,0}$ is discretely divergence-free, one obtains

$$\begin{aligned} a(\mathbf{u}_h, \mathbf{w}_h) &= \frac{1}{\nu} (\mathbf{f}, \Pi(r\mathbf{w}_h))_{L^2} = \frac{1}{\nu} (\mathbb{P}\mathbf{f}, \Pi(r\mathbf{w}_h))_{L^2} \\ &= (\mathbb{P}(-\Delta_{\text{axi}}\mathbf{u}), \Pi(r\mathbf{w}_h))_{L^2} + \nu^{-1} (\nabla\alpha_{\mathbf{f}}, \Pi(r\mathbf{w}_h))_{L^2}. \end{aligned}$$

Due to (3.2) and estimates similar to (3.3), all terms are well-defined. Adding and subtracting $(\mathbb{P}(-\Delta_{\text{axi}}\mathbf{u}), r\mathbf{w}_h)_{L^2}$ yields

$$(3.8) \quad a(\mathbf{u}_h, \mathbf{w}_h) = (\mathbb{P}(-\Delta_{\text{axi}}\mathbf{u}), \Pi(r\mathbf{w}_h) - r\mathbf{w}_h)_{L^2} + (\mathbb{P}(-\nu\Delta_{\text{axi}}\mathbf{u}), \mathbf{w}_h)_{L_1^2} + \nu^{-1} (\nabla\alpha_{\mathbf{f}}, \Pi(r\mathbf{w}_h))_{L^2}.$$

Next note, that we have

$$(3.9) \quad \begin{aligned} (\mathbb{P}(-\nu\Delta_{\text{axi}}\mathbf{u}), \mathbf{w}_h)_{L_1^2} &= (\mathbb{P}(-\nu\Delta_{\text{axi}}\mathbf{u}), \mathbf{w}_h - \mathcal{L}_S \mathbf{w}_h)_{L_1^2} + (\mathbb{P}(-\nu\Delta_{\text{axi}}\mathbf{u}), \mathcal{L}_S \mathbf{w}_h)_{L_1^2} \\ &= (\mathbb{P}(-\nu\Delta_{\text{axi}}\mathbf{u}), \mathbf{w}_h - \mathcal{L}_S \mathbf{w}_h)_{L_1^2} + a(\Pi_S \mathbf{u}, \mathbf{w}_h), \end{aligned}$$

where the last step follows from

$$(\mathbb{P}(-\nu\Delta_{\text{axi}}\mathbf{u}), \mathcal{L}_S \mathbf{w}_h)_{L_1^2} \stackrel{(2.6)}{=} a(\mathbf{u}, \mathcal{L}_S \mathbf{w}_h) \stackrel{(3.4)}{=} a(\Pi_S \mathbf{u}, \mathbf{w}_h).$$

This shows that

$$\begin{aligned} \|\mathbf{w}_h\|_{\mathbf{V}}^2 &= a(\mathbf{w}_h, \mathbf{w}_h) = a(\mathbf{u}_h, \mathbf{w}_h) - a(\Pi_S \mathbf{u}, \mathbf{w}_h) \\ &\stackrel{(3.8)}{=} (\mathbb{P}(-\nu\Delta_{\text{axi}}\mathbf{u}), \Pi(r\mathbf{w}_h) - r\mathbf{w}_h)_{L^2} + (\mathbb{P}(-\nu\Delta_{\text{axi}}\mathbf{u}), \mathbf{w}_h)_{L_1^2} - a(\Pi_S \mathbf{u}, \mathbf{w}_h) \\ &\quad + \nu^{-1} (\nabla\alpha_{\mathbf{f}}, \Pi(r\mathbf{w}_h))_{L^2} \\ &\stackrel{(3.9)}{=} (\mathbb{P}(-\nu\Delta_{\text{axi}}\mathbf{u}), \Pi(r\mathbf{w}_h) - r\mathbf{w}_h)_{L^2} + (\mathbb{P}(-\nu\Delta_{\text{axi}}\mathbf{u}), \mathbf{w}_h - \mathcal{L}_S \mathbf{w}_h)_{L_1^2} \\ &\quad + \nu^{-1} (\nabla\alpha_{\mathbf{f}}, \Pi(r\mathbf{w}_h))_{L^2} \\ &\leq \left(\|\mathbb{P}(\Delta_{\text{axi}}\mathbf{u}) \circ (\mathbb{I} - \Pi)\|_{\mathbf{V}_{h,0}^*} + h^s \|\mathbb{P}(\Delta_{\text{axi}}\mathbf{u})\|_{L_1^2} + \nu^{-1} \|\nabla\alpha_{\mathbf{f}} \circ \Pi\|_{\mathbf{V}_{h,0}^*} \right) \|\mathbf{w}_h\|_{\mathbf{V}}, \end{aligned}$$

which concludes the proof. \square

Remark 3.3 (Lack of pressure-robustness for $\Pi = \mathbb{I}$). While the consistency error $\|\mathbb{P}(\Delta_{\text{axi}}\mathbf{u}) \circ (\mathbb{I} - \Pi)\|_{\mathbf{V}^*}$ in (3.5) vanishes for $\Pi = \mathbb{I}$, the remaining term is only bounded by the best-approximation error in the pressure space

$$(3.10) \quad \|\nabla\alpha_{\mathbf{f}} \circ \Pi\|_{\mathbf{V}_{h,0}^*} = \|\nabla\alpha_{\mathbf{f}}\|_{\mathbf{V}_{h,0}^*} = \inf_{q_h \in Q_h} \|\nabla(\alpha_{\mathbf{f}} - q_h)\|_{\mathbf{V}_{h,0}^*} \lesssim \inf_{q_h \in Q_h} \|\alpha_{\mathbf{f}} - q_h\|_{L_1^2}.$$

Since it appears with the factor ν^{-1} in (3.5), it causes a locking effect in the limit $\nu \rightarrow 0$ if the pressure cannot be approximated well enough. This characterizes the typical non-pressure-robust behavior of classical finite element methods.

Remark 3.4 (Condition for pressure-robustness). To avoid the locking effect outlined in the previous remark, the term (3.10) needs to vanish. To ensure this, a potential reconstruction operator needs to guarantee the pointwise divergence-free condition

$$(3.11) \quad \operatorname{div}(\Pi(r\mathbf{v}_h)) = 0 \quad \text{for all } \mathbf{v}_h \in \mathbf{V}_{h,0}.$$

4. Classical $H(\operatorname{div})$ -conforming reconstruction operators. If the pressure space Q_h consists of piecewise discontinuous polynomials of order $k - 1$, the standard interpolation operators Π_{BDM1} or Π_{RT0} into the Brezzi–Douglas–Marini (BDM) finite element space

$$\text{BDM}_k(\mathcal{T}) := P_k(\mathcal{T}) \cap H(\operatorname{div}, \Omega),$$

or the space of Raviart–Thomas (RT) finite element functions

$$\text{RT}_{k-1}(\mathcal{T}) := \left\{ \mathbf{v}_h \in P_k(\mathcal{T}) \cap \text{BDM}_k(\mathcal{T}) : \forall T \in \mathcal{T} \exists a, b, c \in P_{k-1}(T) : \mathbf{v}_h(r, z)|_T = \begin{pmatrix} a \\ b \end{pmatrix} + c \begin{pmatrix} r \\ z \end{pmatrix} \right\},$$

can be employed. Recall that $H(\operatorname{div}, \Omega)$ -conformity for polynomials requires continuous normal traces over all faces \mathcal{F} of the triangulation.

For these standard interpolations, the following commutative property holds:

$$(4.1) \quad \operatorname{div}_{(r,z)} \Pi(r\mathbf{v}) = \pi_{k-1} \operatorname{div}_{(r,z)}(r\mathbf{v}) \in Q_h \quad \text{for all } \mathbf{v} \in L^2(\Omega) \text{ and } r\mathbf{v} \in H(\operatorname{div}, \Omega),$$

where π_{k-1} is the L^2 -orthogonal projection onto $P_{k-1}(\mathcal{T})$. This directly ensures (3.11). Moreover, first-order approximation properties hold in the sense

$$(4.2) \quad \|(1 - \Pi)\mathbf{v}\|_{L^2} \leq \|h\nabla\mathbf{v}\|_{L^2} \quad \text{for all } \mathbf{v} \in \mathbf{V}.$$

Applied to a weighted test function this yields

$$(4.3) \quad \|(1 - \Pi)(r\mathbf{v})\|_{L^2} \leq \|h\nabla(r\mathbf{v})\|_{L^2} \leq \|hv_r\|_{L^2} + \|hr\nabla\mathbf{v}\|_{L^2} \lesssim h\|\mathbf{v}\|_{\mathbf{V}}.$$

Remark 4.1 (Regularity issue). It is not guaranteed that the continuity estimates (3.2) and (3.3) hold for the standard reconstructions Π_{RT0} and Π_{BDM1} . However, if the right hand side has the (higher) regularity $\mathbf{f} \in L^2(\Omega)$, then we still get

$$(\mathbf{f}, \Pi(r\mathbf{v}_h))_{L^2} \leq \|\mathbf{f}\|_{L^2} \|\Pi(r\mathbf{v}_h)\|_{L^2} \lesssim \|\mathbf{f}\|_{L^2} \|r\mathbf{v}_h\|_{H^1} \lesssim \|\mathbf{f}\|_{L^2} \|\mathbf{v}_h\|_{\mathbf{V}},$$

using the standard properties known from the Cartesian setting, see (4.3). Unfortunately, if only $\mathbf{f} \in L^2_1(\Omega) \setminus L^2(\Omega)$, well-posedness is not guaranteed in general. Indeed, a counter example for (3.2) relies on the fact that the reconstruction $\Pi(r\mathbf{v}_h)$ does not need to vanish at the rotation axis Γ_{rot} . For the function $\mathbf{w}_h := (r, -2z) \in \mathbf{V}_0$ the $\text{RT}_0(\mathcal{T})$ reconstruction of $r\mathbf{w}_h$ must be divergence-free and constant and hence $\Pi_{\text{RT0}}(r\mathbf{w}_h) \in P_0(\mathcal{T})$. At the rotation axis that constant will not be zero in general, which yields $\|\Pi_{\text{RT0}}(r\mathbf{w}_h)\|_{L^2_1} = \infty$.

Besides the regularity issue above, the consistency error in Theorem 3.2 can be estimated for the standard reconstruction operators under slightly larger regularity assumptions on the data.

THEOREM 4.2. *If there holds $\mathbb{P}(\Delta_{\text{axi}}\mathbf{u}) \in L^2(\Omega)$ (which is guaranteed by $\mathbf{f} \in L^2(\Omega)$), the consistency error (3.6) for $\Pi \in \{\Pi_{\text{RT0}}, \Pi_{\text{BDM1}}\}$ can be estimated by*

$$\|\mathbb{P}(\Delta_{\text{axi}}\mathbf{u}) \circ (\mathbb{I} - \Pi)\|_{\mathbf{V}^*} \lesssim \|h_{\mathcal{T}}\mathbb{P}(\Delta_{\text{axi}}\mathbf{u})\|_{L^2}$$

Proof. This follows by applying the Cauchy-Schwarz inequality and (4.3), i.e.,

$$\begin{aligned} (\mathbb{P}(\Delta_{\text{axi}}\mathbf{u}), r\mathbf{w}_h - \Pi(r\mathbf{w}_h))_{L^2} &\leq \|h_{\mathcal{T}}\mathbb{P}(\Delta_{\text{axi}}\mathbf{u})\|_{L^2} \|h_{\mathcal{T}}^{-1}(1 - \Pi)(r\mathbf{w}_h)\|_{L^2} \\ &\lesssim \|h_{\mathcal{T}}\mathbb{P}(\Delta_{\text{axi}}\mathbf{u})\|_{L^2} \|\mathbf{w}_h\|_{\mathbf{V}}. \end{aligned} \quad \square$$

Remark 4.3. To solve the regularity issue, we could try to look for a reconstruction operator acting on \mathbf{v} instead of $r\mathbf{v}$. A possible choice is an operator from [5] for an axisymmetric Maxwell problem, which (adapted to our setting) reads as

$$\tilde{\Pi}_{\text{RT0}}(\mathbf{v}) := \sum_{E \in \mathcal{E}} \psi_E^{\text{RT0}} \frac{\int_E \mathbf{v} \cdot \mathbf{n} r ds}{\int_E r ds},$$

where ψ_E^{RT0} is the RT₀ basis functions for the edge $E \in \mathcal{E}$. While $r\tilde{\Pi}_{\text{RT0}}(\mathbf{v}) \neq \Pi_{\text{RT0}}(r\mathbf{v})$, the operators satisfy

$$\begin{aligned} \int_T \operatorname{div}_{(r,z)}(\tilde{\Pi}_{\text{RT0}}(\mathbf{v})r) dx &= \int_{\partial T} \tilde{\Pi}_{\text{RT0}}(\mathbf{v}) \cdot \mathbf{n} r ds = \int_{\partial T} \mathbf{v} \cdot \mathbf{n} r ds \\ &= \int_T \operatorname{div}_{(r,z)}(\Pi_{\text{RT0}}(r\mathbf{v})) ds = \int_T \operatorname{div}_{(r,z)}(r\mathbf{v}) ds, \end{aligned}$$

or, in other words,

$$\operatorname{div}_{(r,z)}(\Pi_{\text{RT0}}(r\mathbf{v})) = \pi_0(\operatorname{div}_{(r,z)}(r\mathbf{v})) = \pi_0(\operatorname{div}_{(r,z)}(\tilde{\Pi}_{\text{RT0}}(\mathbf{v})r)).$$

Unfortunately, it holds $\operatorname{div}_{(r,z)}(\tilde{\Pi}_{\text{RT0}}(\mathbf{v})r) \notin Q_h$ in general, so using $\tilde{\Pi}_{\text{RT0}}(\mathbf{v})r$ in the right-hand side would probably solve the regularity issue (see [5, Lemma 5.3]), but will not result in a pressure-robust discretization requiring $\operatorname{div}_{(r,z)}(\Pi(\mathbf{v}r)) \in Q_h$.

5. A modified reconstruction operator. This section presents a design for a modified reconstruction operator that ensures pointwise homogeneous boundary conditions along Γ_{rot} . This condition is the key to get a reconstruction operator that maps $r\mathbf{u} \in H_{-1}(\operatorname{div}, \Omega)$ into an $L_{-1}^2(\Omega)$ -conforming discrete subspace of $H(\operatorname{div}, \Omega)$, see (2.4). The slightly more involved construction allows to lower the regularity assumptions on $\mathbb{P}(\Delta_{\text{axi}}\mathbf{u})$ in the consistency error estimate. In comparison to (4.3), the improved error estimate

$$(5.1) \quad \|(1 - \Pi)(r\mathbf{v})\|_{L_{-1}^2} \lesssim h \|\mathbf{v}\|_{\mathbf{V}},$$

is shown in Theorem 5.3 below. The novel design only requires a modification of some ansatz functions close to the rotation axis Γ_{rot} .

5.1. Modified $L_{-1}^2(\Omega) \cap H(\operatorname{div}, \Omega)$ -conforming interpolation. For any triangle $T \in \mathcal{T}$, let $\mathcal{E}(T)$ be the set of all edges of T . We define the set

$$(5.2) \quad \mathcal{E}_R := \{E \in \mathcal{E} : E \cap \Gamma_{\text{rot}} \neq \emptyset, E \not\subseteq \Gamma_{\text{rot}}\},$$

collecting all interior edges that have one vertex on the rotation axis. In Figure 3, we show that there are two possible types of triangles appearing on the rotation axis, which require special care in some parts of the analysis for weighted Sobolev norms.

We are interested in a reconstruction operator that maps into the space of piecewise linear functions that vanish at the rotation axis, and which is $H(\operatorname{div})$ -conforming in the sense of normal-continuity. In this case, considering a type 2 triangle, such a polynomial must have the form $r\mathbf{P}_0(T)$. Unfortunately, this is not a classical lowest order Raviart–Thomas function (if it is non-zero), but motivates to extend the space by certain polynomial functions. In the following, we design a suitable reconstruction operator based on modified Raviart–Thomas basis functions, which can be understood as a constrained BDM₁ space.

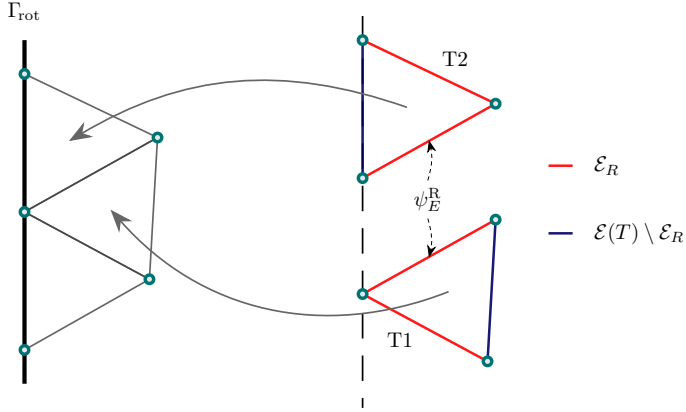


Figure 3: We distinguish between type 2 (T2) with two vertices on the rotation axis Γ_{rot} and type 1 (T1) triangles with one vertex on the rotation axis Γ_{rot} . Both types of triangles have two edges belonging to \mathcal{E}_R on which we define a modified basis function ψ_E^R in (5.3).

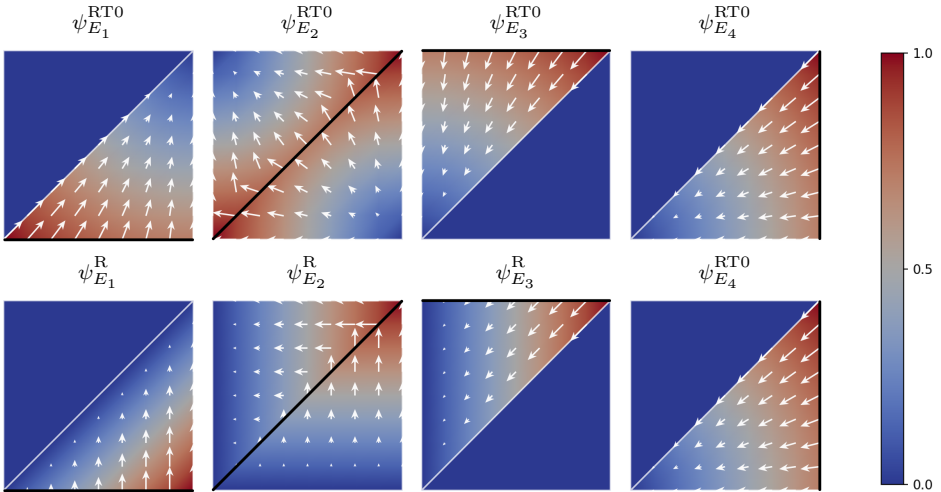


Figure 4: Top row: Standard Raviart–Thomas basis functions on a simple two element mesh (Γ_{rot} corresponds to the left edge). Bottom row: Modified Raviart–Thomas basis functions. Edges corresponding to the shape functions are highlighted. The color encodes the normalized magnitude.

Consider an edge $E = \text{conv}\{P_i, P_j\} \in \mathcal{E}_R$ with vertex $P_j = (r_j, z_j) \in \Gamma_{\text{rot}}$ on the rotation axis (recall that both type 1 and type 2 triangles have two of them). For this edge E , we define a modified RT_0 function by

$$(5.3) \quad \psi_E^R := 2\text{curl}(\lambda_j)\lambda_i,$$

where λ_i and λ_j are the standard barycentric coordinates associated to the vertices

P_i and P_j , respectively. It can be obtained by a linear combination of the standard RT_0 and BDM_1 basis functions which (up to scaling factors) usually have the form

$$\psi_E^{\text{RT0}} := \text{curl}(\lambda_i)\lambda_j - \text{curl}(\lambda_j)\lambda_i \quad \text{and} \quad \psi_E^{\text{BDM1}} := \text{curl}(\lambda_i\lambda_j).$$

Figure 4 displays the four classical and the four modified Raviart–Thomas basis functions on a triangulation with two triangles, one type 1 and one type 2 triangle. Observe how all modified basis functions vanish at the rotation axis on the left. The following lemma collects some useful properties of the modified basis functions.

LEMMA 5.1 (Properties of modified basis functions). *The function (5.3) for an edge $E = \text{conv}\{P_i, P_j\} \in \mathcal{E}_R$ with $P_j \in \Gamma_{\text{rot}}$ and $P_i \notin \Gamma_{\text{rot}}$ has the following properties:*

- (i) $\int_E \psi_E^{\text{R}} \cdot \mathbf{n} \, ds = \pm 1$ (sign depends on orientation of \mathbf{n}),
- (ii) $\int_{\tilde{E}} \psi_E^{\text{R}} \cdot \mathbf{n} \, ds = 0$ for all other edges $\tilde{E} \in \mathcal{E}$ with $\tilde{E} \neq E$,
- (iii) $\psi_E^{\text{R}}(P_j) = 0$,
- (iv) $\|\psi_E^{\text{R}}\|_{L^2_{-1}(T)} \lesssim h_T^{-1/2}$.

Moreover, in a type 1 triangle on the edge $E \in \mathcal{E}(T) \setminus \mathcal{E}_R$ away from the rotation axis, it also holds

- (v) $\|\psi_E^{\text{RT0}}\|_{L^2_{-1}(T)} \lesssim h_T^{-1/2}$,
- (vi) $\|\psi_E^{\text{BDM1}}\|_{L^2_{-1}(T)} \lesssim h_T^{-1/2}$.

On triangles T with no vertex on the rotation axis, it holds $\|\psi_E^{\text{RT0}}\| \approx 1 \approx \|\psi_E^{\text{BDM1}}\|$.

Proof. The first three properties follow from straightforward calculations. For property (iv), let z_j be the z -coordinate of the vertex $P_j \in \Gamma_{\text{rot}}$. Then the value λ_i at a point (r, z) can be expressed as $\lambda_i = \nabla \lambda_i \cdot (r, z - z_j)$, because λ_i is zero at the vertex P_j . This gives

$$\begin{aligned} \|\psi_E^{\text{R}}\|_{L^2_{-1}(T)}^2 &= 4|\text{curl}(\lambda_j)|^2 \int_T \frac{\lambda_i^2}{r} \, dr dz \\ &= 4|\text{curl}(\lambda_j)|^2 \int_T \frac{(\nabla \lambda_i \cdot (r, z - z_j))^2}{r} \, dr dz \\ &\leq 4|\text{curl}(\lambda_j)|^2 |\nabla(\lambda_j)|^2 \int_T \frac{r^2 + (z - z_j)^2}{r} \, dr dz. \end{aligned}$$

The last integral can be transformed with the transformation $(r, z - z_j) = \Phi(r, \alpha) = (r, r \sin(\alpha))$ and $\det(D\Phi) = r \cos(\alpha)$, where $\alpha \in [\alpha_{\min}, \alpha_{\max}]$ is the angle between the r -axis and the line connecting the point $(r, z) \in T$ with the vertex P_j . Then we obtain

$$\begin{aligned} \int_T \frac{r^2 + (z - z_j)^2}{r} \, dr dz &= \int_{\alpha_{\min}}^{\alpha_{\max}} \int_0^{R(\alpha)} r^2 (1 + \sin(\alpha))^2 \cos(\alpha) \, dr d\alpha \\ &\leq \max_{\alpha \in (\alpha_{\min}, \alpha_{\max})} |1 + \sin(\alpha)|^2 h_T^3. \end{aligned}$$

The proof of (v) and (vi) is very similar to the proof of (iv). This concludes the proof. \square

DEFINITION 5.2 (Modified interpolation operators). *We recall the definition of the set \mathcal{E}_R in (5.2) for which the modified basis functions shall be used. Then we define the space*

$$\text{RT}_0^{\text{axi}}(\mathcal{T}) := \text{span} \left[\left\{ \psi_E^{\text{R}} : E \in \mathcal{E}_R \right\} \cup \left\{ \psi_E^{\text{RT0}} : E \in \mathcal{E} \setminus \mathcal{E}_R \right\} \right],$$

where linear independency follows from property (i) and (ii) of Lemma 5.1. Further, we define the space spans the space

$$\begin{aligned} \text{BDM}_1^{\text{axi}}(\mathcal{T}) &:= \text{RT}_0^{\text{axi}}(\mathcal{T}) \cup \text{span} \left\{ \psi_E^{\text{BDM1}} : E \in \mathcal{E} \setminus \mathcal{E}_R \right\} \\ &= \left\{ \mathbf{v}_h \in \text{BDM}_1(\mathcal{T}) : \mathbf{v}_h = \mathbf{0} \text{ on } \Gamma_{\text{rot}} \right\}. \end{aligned}$$

The modified interpolations $\Pi_{\text{RT0}}^{\text{axi}} : \mathbf{V} \rightarrow \text{RT}_0^{\text{axi}}(\mathcal{T})$ and $\Pi_{\text{BDM1}}^{\text{axi}} : \mathbf{V} \rightarrow \text{BDM}_1^{\text{axi}}(\mathcal{T})$ of some function $\mathbf{w} \in \mathbf{V}$ are uniquely characterized by

$$\int_E (\Pi_{\text{RT0}}^{\text{axi}} \mathbf{w} - \mathbf{w}) \cdot \mathbf{n} \, ds = 0 \quad \text{for all } E \in \mathcal{E},$$

and

$$\begin{aligned} \int_E (\Pi_{\text{BDM1}}^{\text{axi}} \mathbf{w} - \mathbf{w}) \cdot \mathbf{n} \, ds &= 0 \quad \text{for all } E \in \mathcal{E}_R, \\ \int_E (\Pi_{\text{BDM1}}^{\text{axi}} \mathbf{w} - \mathbf{w}) \cdot \mathbf{n} r_h \, ds &= 0 \quad \text{for all } E \in \mathcal{E} \setminus \mathcal{E}_R, r_h \in P_1(E). \end{aligned}$$

5.2. Improved consistency error estimate. The modifications allow for the following improved interpolation estimate for $\Pi_{\text{RT0}}^{\text{axi}}$ (and analogously for $\Pi_{\text{BDM1}}^{\text{axi}}$).

THEOREM 5.3 (L_{-1}^2 interpolation error estimate for $\Pi_{\text{RT0}}^{\text{axi}}$). *For a function $\mathbf{v} \in \mathbf{H}_1^1(T)$ with $v_r \in L_{-1}^2(T)$ on a type 1 or type 2 triangle, it holds*

$$\|r\mathbf{v} - \Pi_{\text{RT0}}^{\text{axi}}(r\mathbf{v})\|_{L_{-1}^2(T)} \lesssim h_T^{3/2} \|\mathbf{v}\|_{\mathbf{V}}.$$

Globally, there holds

$$\|h_{\mathcal{T}}^{-1} (r\mathbf{v} - \Pi_{\text{RT0}}^{\text{axi}}(r\mathbf{v}))\|_{L_{-1}^2(\Omega)} \lesssim \|\mathbf{v}\|_{\mathbf{V}}.$$

Proof. For triangles that are not of type 1 or type 2, the estimate follows from the usual RT_0 interpolation estimates (scaled by $r_{\max}/r_{\min} \approx 1$) with order h instead of $h^{3/2}$. Hence, the proof concentrates on type 1 or type 2 triangles, such that the modified basis functions are involved.

For any constant $\mathbf{v}_T := (0, v_{T,z}) \in \mathbf{P}_0(T)$, the Friedrichs inequality and the product rule yields

$$(5.4) \quad \|r(\mathbf{v} - \mathbf{v}_T)\|_{L_{-1}^2(T)} = \|\mathbf{v} - \mathbf{v}_T\|_{L_1^2(T)} \lesssim h_T \|\nabla(r^{1/2}(\mathbf{v} - \mathbf{v}_T))\|_{L^2(T)} \lesssim h_T \|\mathbf{v}\|_{\mathbf{V}}.$$

Since $\Pi_{\text{RT0}}^{\text{axi}}$ interpolates constants exactly, a triangle inequality yields

$$\|r\mathbf{v} - \Pi_{\text{RT0}}^{\text{axi}}(r\mathbf{v})\|_{L_{-1}^2(T)} \leq \|\mathbf{v} - \mathbf{v}_T\|_{L_1^2(T)} + \|\Pi_{\text{RT0}}^{\text{axi}}(r(\mathbf{v} - \mathbf{v}_T))\|_{L_{-1}^2(T)}.$$

The basis representation of the modified RT_0 interpolation reads

$$\begin{aligned} &\Pi_{\text{RT0}}^{\text{axi}}(r(\mathbf{v} - \mathbf{v}_T)) \\ &= \sum_{E \in \mathcal{E}(T) \cap \mathcal{E}_R} \left(\int_E r(\mathbf{v} - \mathbf{v}_T) \cdot \mathbf{n} \, ds \right) \psi_E^{\text{R}} + \sum_{E \in \mathcal{E}(T) \setminus \mathcal{E}_R} \left(\int_E r(\mathbf{v} - \mathbf{v}_T) \cdot \mathbf{n} \, ds \right) \psi_E^{\text{RT0}}. \end{aligned}$$

Due to property (iv) in Lemma 5.1 for $\|\psi_E^R\|_{L_{-1}^2}$, it remains to bound the coefficients. The trace identity (which follows from integration by parts) reads

$$\begin{aligned} & \int_E r(\mathbf{v} - \mathbf{v}_T) \cdot \mathbf{n} \, ds \\ &= \frac{|E|}{|T|} \int_T r(\mathbf{v} - \mathbf{v}_T) \cdot \mathbf{n} \, drdz + \frac{|E|}{2|T|} \int_T \nabla(r(\mathbf{v} - \mathbf{v}_T) \cdot \mathbf{n}) \cdot (\mathbf{x} - \mathbf{x}_E) \, drdz, \end{aligned}$$

where $\mathbf{x}_E = (x_{E,r}, x_{E,z})$ is the vertex in T opposite to E , and the normal vector \mathbf{n} associated to the edge E is constantly extended on T . An application of the Cauchy-Schwarz inequality, the Friedrichs inequality (5.4), and $r \leq h_T$ show

$$\int_T r(\mathbf{v} - \mathbf{v}_T) \cdot \mathbf{n} \, drdz \leq \|1\|_{L_1^2(T)} \|\mathbf{v} - \mathbf{v}_T\|_{L_1^2(T)} \lesssim h_T^{5/2} \|\mathbf{v}\|_{\mathbf{V}},$$

and the product rule $\nabla(r(\mathbf{v} - \mathbf{v}_T) \cdot \mathbf{n}) = r\nabla(\mathbf{v} \cdot \mathbf{n}) + (\mathbf{v} - \mathbf{v}_T) \cdot \mathbf{n}\nabla r$ yields

$$\begin{aligned} & \int_T \nabla(r(\mathbf{v} - \mathbf{v}_T) \cdot \mathbf{n}) \cdot (\mathbf{x} - \mathbf{x}_E) \, drdz \\ & \leq \|\nabla\mathbf{v}\|_{L_1^2(T)} \|\mathbf{x} - \mathbf{x}_E\|_{L_1^2(T)} + \int_T (\mathbf{v} - \mathbf{v}_T) \cdot \mathbf{n} (r - x_{E,r}) \, drdz. \end{aligned}$$

Next we observe that on the two edges of a type 2 triangle or on the edge opposite to the rotation axis (i.e. that has no vertex on Γ) in a type 1 triangle, the r -component $x_{E,r}$ of \mathbf{x}_E vanishes since $\mathbf{x}_E \in \Gamma$ and thus $\int_T (\mathbf{v} - \mathbf{v}_T) \cdot \mathbf{n} x_{E,r} \, drdz = 0$. For the remaining cases, i.e. when we consider an edge E of a type 1 triangle that has one vertex on Γ_{rot} , it holds $n_z \neq 0$ and we can choose $v_{T,z}$ such that again $\int_T (\mathbf{v} - \mathbf{v}_T) \cdot \mathbf{n} x_{E,r} \, drdz = 0$. For all cases one obtains

$$\begin{aligned} \int_T (\mathbf{v} - \mathbf{v}_T) \cdot \mathbf{n} (r - x_{E,r}) \, drdz &= \int_T (\mathbf{v} - \mathbf{v}_T) \cdot \mathbf{n} r \, drdz \lesssim \|\mathbf{v} - \mathbf{v}_T\|_{L_1^2(T)} \|1\|_{L_1^2(T)} \\ &\lesssim h_T^{5/2} \|\mathbf{v}\|_{\mathbf{V}}. \end{aligned}$$

Since also $\|\mathbf{x} - \mathbf{x}_E\|_{L_1^2(T)} \leq h_T \|1\|_{L_1^2(T)} \lesssim h_T^{5/2}$, this yields

$$\int_T \nabla(r(\mathbf{v} - \mathbf{v}_T) \cdot \mathbf{n}) \cdot (\mathbf{x} - \mathbf{x}_E) \, drdz \lesssim h_T^{5/2} \|\mathbf{v}\|_{\mathbf{V}}.$$

Eventually, one obtains the final estimate

$$\|\Pi_{\text{RT0}}^{\text{axi}}(r(\mathbf{v} - \mathbf{v}_T))\|_{L_{-1}^2(T)} \lesssim \sum_{E \in \mathcal{E}_R \cap \mathcal{E}(T)} \left| \int_E r(\mathbf{v} - \mathbf{v}_T) \cdot \mathbf{n} \, ds \right| \|\psi_E^R\|_{L_{-1}^2} \lesssim h_T^{3/2} \|\mathbf{v}\|_{\mathbf{V}},$$

which concludes the proof. \square

Finally, the modified interpolation estimate allows to show the following improved consistency error estimate for $\Pi_{\text{RT0}}^{\text{axi}}$ (and analogously for $\Pi_{\text{BDM1}}^{\text{axi}}$).

THEOREM 5.4. *If $\mathbf{f} \in L_1^2(\Omega)$ (and hence $\mathbb{P}(\Delta_{\text{axi}}\mathbf{u}) \in L_1^2(\Omega)$), the consistency error (3.6) for $\Pi \in \{\Pi_{\text{RT0}}^{\text{axi}}, \Pi_{\text{BDM1}}^{\text{axi}}\}$ can be estimated by*

$$\|\mathbb{P}(\Delta_{\text{axi}}\mathbf{u}) \circ (\mathbb{I} - \Pi)\|_{\mathbf{V}^*} \lesssim \|h_{\mathcal{T}}\mathbb{P}(\Delta_{\text{axi}}\mathbf{u})\|_{L_1^2}.$$

Proof. This follows directly by applying the Cauchy-Schwarz inequality and Theorem 5.3, i.e.,

$$\begin{aligned} (\mathbb{P}(\Delta_{\text{axi}}\mathbf{u}), r\mathbf{w}_h - \Pi(r\mathbf{w}_h))_{L^2} &\leq \|h_{\mathcal{T}}\mathbb{P}(\Delta_{\text{axi}}\mathbf{u})\|_{L^2_1} \|h_{\mathcal{T}}^{-1}(1 - \Pi)(r\mathbf{w}_h)\|_{L^2_{-1}} \\ &\lesssim \|h_{\mathcal{T}}\mathbb{P}(\Delta_{\text{axi}}\mathbf{u})\|_{L^2_1} \|\mathbf{w}_h\|_{\mathbf{V}}. \end{aligned} \quad \square$$

6. Numerical examples. This section compares a classical Bernardi–Raugel (BR) finite element discretization with a pressure-robustly modified discretization with $\Pi \in \{\Pi_{\text{RT0}}^{\text{axi}}, \Pi_{\text{BDM1}}^{\text{axi}}\}$. If not mentioned otherwise the right-hand side functionals and boundary data integrals are evaluated with a quadrature rule of order 10, while the bilinear form a is evaluated with a quadrature rule of order 4. The used grids are unstructured triangular grids without any refinement close to the rotation axis.

6.1. Example 1: linear stagnation flow. As a first example, we consider the axisymmetric Stokes problem with the exact solutions and data

$$p_{\text{ex}} = r^{7/4} + z^2, \quad \mathbf{u}_{\text{ex}} = [r, -2z]^T, \quad \mathbf{f} = -\nu\Delta_{\text{axi}}\mathbf{u}_{\text{ex}} + \nabla p_{\text{ex}}.$$

Observe, that $\Delta_{\text{axi}}\mathbf{u}_{\text{ex}} = \mathbf{0}$ and $\nabla p_{\text{ex}} \in L^2(\Omega)$, and in particular, the exact velocity solution is in the discrete ansatz space of the BR finite element method.

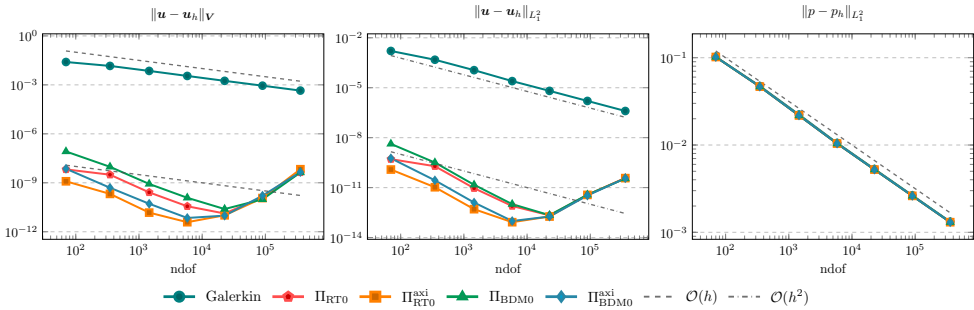


Figure 5: Error convergence histories in Example 1 for $\nu = 1$.

Figure 5 shows that indeed all variants that use one of the suggested reconstruction operators, have errors close to zero, while the classical BR finite element method without the reconstruction operator shows errors in the range of the pressure best-approximation error. Note that this error scales with ν^{-1} , which is demonstrated in the next examples.

6.2. Example 2: smooth example. We consider an example with smooth data, where we expect all methods to show optimal convergence rates. Specifically, we choose

$$p_{\text{ex}} = \sin(\pi(r^2 + z^2)), \quad \mathbf{u}_{\text{ex}} = \begin{pmatrix} r^3 \sin z \\ 4r^2 \cos z \end{pmatrix}, \quad \mathbf{f} = -\nu\Delta_{\text{axi}}\mathbf{u}_{\text{ex}} + \nabla p_{\text{ex}}.$$

Figure 6 shows the convergence history for several norms of interest for $\nu = 10^{-3}$. In the energy and L^2_1 error of $\mathbf{u} - \mathbf{u}_h$ all variants of the reconstruction operators perform equally well and the classical BR finite element method shows larger errors by about two orders of magnitude. As expected, the L^2_{-1} error of $r\mathbf{u} - \Pi(r\mathbf{u}_h)$ converges

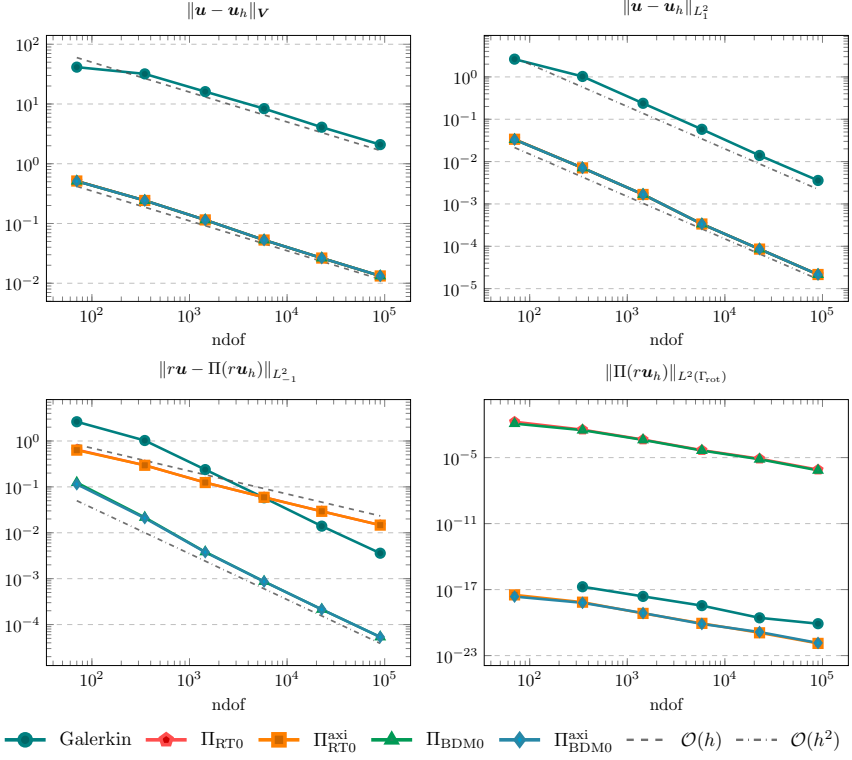


Figure 6: Error convergence histories in Example 2 for $\nu = 10^{-3}$.

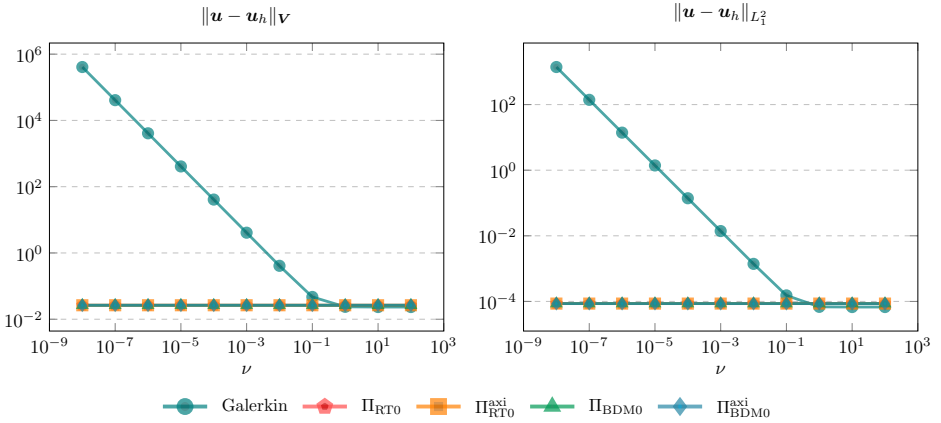


Figure 7: Error convergence histories in Example 2 with respect to variable ν on a fixed mesh with about 22,000 degrees of freedom.

only linearly for Π_{RT0} and Π_{RT0}^{axi} , while the BDM1 variants show optimal quadratic convergence and much smaller errors than the Galerkin method. This is of relevance when the reconstruction operator is used as a postprocessing in coupled transport [7]. The last subplot for the norm $\|\Pi(ru_h)\|_{L^2(\Gamma_{rot})}$ confirms that the modified recon-

structured functions really vanish at the rotation axis. However, at least in this smooth example, this property seems to have no qualitative impact on the convergence of the other norms.

Figure 7 shows errors on a fixed mesh but for different values of ν . The plots confirm the locking behavior of the classical method in the sense that at some point the errors scale like ν^{-1} . All modified methods show no locking behavior even for very small viscosities ν .

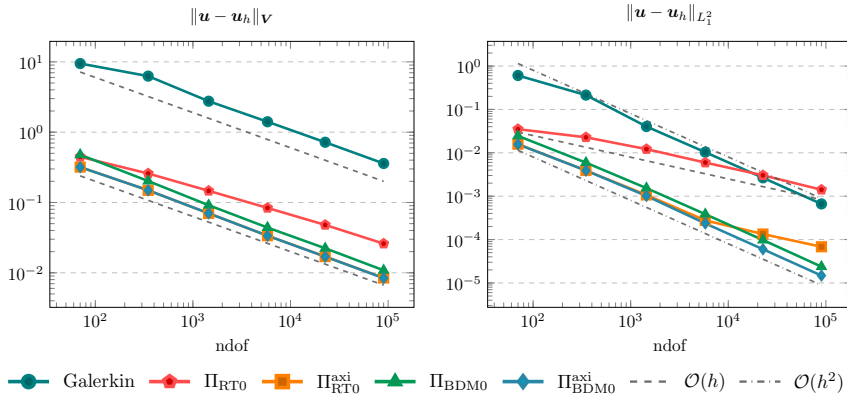


Figure 8: Error convergence histories in Example 3 for $\nu = 10^{-3}$.

6.3. Example 3: data in $L^2_1(\Omega) \setminus L^2(\Omega)$. This example studies the axisymmetric Stokes problem for

$$p_{\text{ex}} = r^{1/2} - \frac{8}{9}, \quad \mathbf{u}_{\text{ex}} = \begin{pmatrix} r^{2.1} \\ -3.1r^{1.1}z \end{pmatrix}, \quad \mathbf{f} = -\nu \Delta_{\text{axi}} \mathbf{u}_{\text{ex}} + \nabla p_{\text{ex}}.$$

Here, it holds $\mathbf{u}_{\text{ex}} \in \mathbf{V}$ and $p \in L^2_1(\Omega)$, but $\mathbf{f} \in L^2_1(\Omega) \setminus L^2(\Omega)$. In other words, the assumptions for the consistency error estimates in Theorem 4.2 are not satisfied, while the ones in Theorem 5.4 are satisfied. In Figure 8, we compare the convergence rates for the fixed parameter $\nu = 10^{-3}$ in the velocity norms. This time, the errors with the classical reconstruction Π_{RT0} are much larger than of the other reconstruction operators. Also with Π_{BDM1} the energy errors are not as small as with the modified reconstruction operators Π_{RT0}^{axi} and Π_{BDM1}^{axi} . Interestingly, the L^2_1 velocity error converges suboptimally for Π_{RT0}^{axi} . This was not the case in the smooth example.

Figure 9 shows the dependency of the error norms on the viscosity ν on a fixed mesh. While the results are very similar for the classical method, there are some interesting differences among the methods with reconstruction operator. First of all, all methods show an increase of the error that scales with ν^{-1} below some critical value for ν . This is related to the quadrature error in the right-hand side and an expected behavior that does not contradict pressure robustness, since Theorem 3.2 assumes exact evaluation of all integrals. In the previous example the data was very smooth, so the quadrature error was small. Due to the lower regularity of the data in this example the quadrature error is much more important.

However, it is interesting that the critical value for the modified reconstruction operators is much smaller than that for the classical reconstruction operators for the

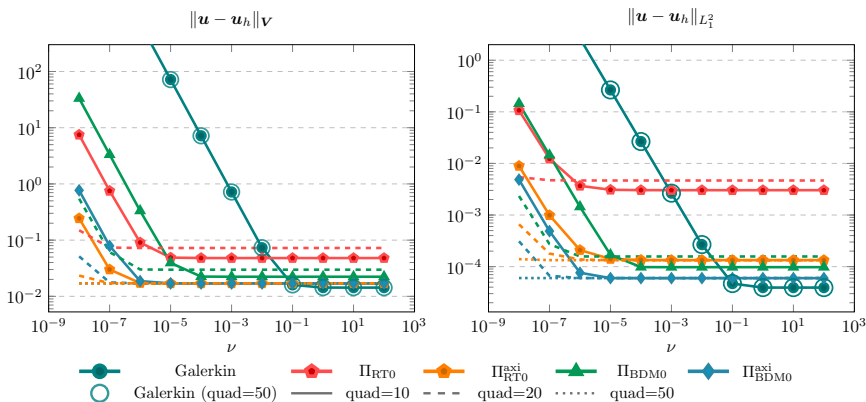


Figure 9: Error convergence histories in Example 2 with respect to variable ν on a fixed mesh for quadrature rules of increasing orders 10, 20, and 50.

same quadrature rule and that seems to be related to the properties of the reconstruction operator. More importantly, it can be observed that the classical reconstruction operator Π_{RT0} yields much larger errors than the Galerkin method for moderate ν .

REFERENCES

- [1] C. BERNARDI, M. DAUGE, AND Y. MADAY, *Spectral methods for axisymmetric domains*, vol. 3 of Series in Applied Mathematics (Paris), Gauthier-Villars, Éditions Scientifiques et Médicales Elsevier, Paris; North-Holland, Amsterdam, 1999. Numerical algorithms and tests due to Mejdí Azaïez.
- [2] C. BERNARDI AND G. RAUGEL, *Analysis of some finite elements for the Stokes problem*, Math. Comp., 44 (1985), pp. 71–79, <https://doi.org/10.2307/2007793>, <https://doi.org/10.2307/2007793>.
- [3] B. BERNSTEIN, K. A. FEIGL, AND E. T. OLSEN, *A first-order exactly incompressible finite element for axisymmetric fluid flow*, SIAM Journal on Numerical Analysis, 33 (1996), pp. 1736–1758, <https://doi.org/10.1137/S0036142994243095>.
- [4] B. COCKBURN, G. KANSCHAT, AND D. SCHÖTZAU, *A note on discontinuous Galerkin divergence-free solutions of the Navier-Stokes equations*, J. Sci. Comput., 31 (2007), pp. 61–73, <https://doi.org/10.1007/s10915-006-9107-7>, <https://doi.org/10.1007/s10915-006-9107-7>.
- [5] D. M. COPELAND, J. GOPALAKRISHNAN, AND J. E. PASCIAK, *A mixed method for axisymmetric div-curl systems*, Math. Comp., 77 (2008), pp. 1941–1965, <https://doi.org/10.1090/S0025-5718-08-02102-9>, <https://doi.org/10.1090/S0025-5718-08-02102-9>.
- [6] M. COSTABEL, M. DAUGE, AND J.-Q. HU, *Characterization of Sobolev spaces by their Fourier coefficients in axisymmetric domains*, Calcolo, 60 (2023), p. 15, <https://doi.org/10.1007/s10092-023-00504-w>, <https://doi.org/10.1007/s10092-023-00504-w>.
- [7] J. FUHRMANN, C. MERDON, AND D. RUNGE, *Axisymmetric mass conservative coupling of fluid flow and solute transport*, 2026.
- [8] J. GOPALAKRISHNAN, P. L. LEDERER, AND J. SCHÖBERL, *A mass conserving mixed stress formulation for the Stokes equations*, IMA Journal of Numerical Analysis, 40 (2020), pp. 1838–1874, <https://doi.org/10.1093/imanum/drz022>, [10.1093/imanum/drz022](https://doi.org/10.1093/imanum/drz022).
- [9] V. JOHN, A. LINKE, C. MERDON, M. NEILAN, AND L. G. REBHOLZ, *On the divergence constraint in mixed finite element methods for incompressible flows*, SIAM Rev., 59 (2017), pp. 492–544, <https://doi.org/10.1137/15M1047696>, <https://doi.org/10.1137/15M1047696>.
- [10] A. KUFNER, *Weighted Sobolev spaces*, vol. 31 of Teubner-Texte zur Mathematik [Teubner Texts in Mathematics], BSB B. G. Teubner Verlagsgesellschaft, Leipzig, 1980. With German, French and Russian summaries.
- [11] P. L. LEDERER, A. LINKE, C. MERDON, AND J. SCHÖBERL, *Divergence-free reconstruction operators for pressure-robust Stokes discretizations with continuous pressure finite elements*,

- SIAM J. Numer. Anal., 55 (2017), pp. 1291–1314, <https://doi.org/10.1137/16M1089964>, <http://dx.doi.org/10.1137/16M1089964>.
- [12] Y.-J. LEE AND H. LI, *On stability, accuracy, and fast solvers for finite element approximations of the axisymmetric Stokes problem by Hood–Taylor elements*, SIAM Journal on Numerical Analysis, 49 (2011), pp. 668–691, <https://doi.org/10.1137/100783339>.
- [13] Y.-J. LEE AND H. LI, *Axisymmetric Stokes equations in polygonal domains: Regularity and finite element approximations*, Computers & Mathematics with Applications, 64 (2012), pp. 3500–3521, <https://doi.org/https://doi.org/10.1016/j.camwa.2012.08.014>, <https://www.sciencedirect.com/science/article/pii/S0898122112005640>.
- [14] C. LEHRENFELD AND J. SCHÖBERL, *High order exactly divergence-free hybrid discontinuous Galerkin methods for unsteady incompressible flows*, Computer Methods in Applied Mechanics and Engineering, 307 (2016), pp. 339 – 361, <https://doi.org/http://dx.doi.org/10.1016/j.cma.2016.04.025>, <http://www.sciencedirect.com/science/article/pii/S004578251630264X>.
- [15] A. LINKE, *On the role of the Helmholtz decomposition in mixed methods for incompressible flows and a new variational crime*, Comput. Methods Appl. Mech. Engrg., 268 (2014), pp. 782–800, <https://doi.org/10.1016/j.cma.2013.10.011>, <https://doi.org/10.1016/j.cma.2013.10.011>.
- [16] A. LINKE, G. MATTHIES, AND L. TOBISKA, *Robust arbitrary order mixed finite element methods for the incompressible Stokes equations with pressure independent velocity errors*, ESAIM Math. Model. Numer. Anal., 50 (2016), pp. 289–309, <https://doi.org/10.1051/m2an/2015044>, <https://doi.org/10.1051/m2an/2015044>.
- [17] A. LINKE AND C. MERDON, *Pressure-robustness and discrete Helmholtz projectors in mixed finite element methods for the incompressible Navier-Stokes equations*, Comput. Methods Appl. Mech. Engrg., 311 (2016), pp. 304–326, <https://doi.org/10.1016/j.cma.2016.08.018>, <https://doi.org/10.1016/j.cma.2016.08.018>.
- [18] A. LINKE, C. MERDON, AND M. NEILAN, *Pressure-robustness in quasi-optimal a priori estimates for the Stokes problem*, Electron. Trans. Numer. Anal., 52 (2020), pp. 281–294, <https://doi.org/10.1553/etna.vol52s281>, <https://doi.org/10.1553/etna.vol52s281>.
- [19] X. LIU, R. ZHANG, S. ZHANG, AND Z. ZHANG, *Rectangular divergence-free finite elements for axisymmetric Stokes equations*, Journal of Scientific Computing, 105 (2025), <https://doi.org/10.1007/s10915-025-03094-7>.
- [20] J. QUERALES, R. RODRÍGUEZ, AND P. VENEGAS, *Numerical approximation of the displacement formulation of the axisymmetric acoustic vibration problem*, SIAM Journal on Scientific Computing, 43 (2021), pp. A1583–A1606, <https://doi.org/10.1137/20M1346225>.
- [21] S. RHEBERGEN AND G. N. WELLS, *A hybridizable discontinuous Galerkin method for the Navier-Stokes equations with pointwise divergence-free velocity field*, J. Sci. Comput., 76 (2018), pp. 1484–1501, <https://doi.org/10.1007/s10915-018-0671-4>, <https://doi.org/10.1007/s10915-018-0671-4>.
- [22] V. RUAS, *Mixed finite element methods with discontinuous pressures for the axisymmetric Stokes problem*, ZAMM Z. Angew. Math. Mech., 83 (2003), pp. 249–264, <https://doi.org/10.1002/zamm.200310032>, <https://doi.org/10.1002/zamm.200310032>.
- [23] L. R. SCOTT AND M. VOGELIUS, *Norm estimates for a maximal right inverse of the divergence operator in spaces of piecewise polynomials*, RAIRO Modél. Math. Anal. Numér., 19 (1985), pp. 111–143, <https://doi.org/10.1051/m2an/1985190101111>, <https://doi.org/10.1051/m2an/1985190101111>.
- [24] S. ZHANG, *Divergence-free finite elements on tetrahedral grids for $k \geq 6$* , Math. Comp., 80 (2011), pp. 669–695, <https://doi.org/10.1090/S0025-5718-2010-02412-3>, <https://doi.org/10.1090/S0025-5718-2010-02412-3>.